

# Analysis of thick composite laminates using a higher-order shear and normal deformable plate theory (HOSNDPT) and a meshless method

J.R. Xiao <sup>a,\*</sup>, D.F. Gilhooley <sup>a,e,g</sup>, R.C. Batra <sup>d</sup>, J.W. Gillespie Jr. <sup>a,b,c</sup>, M.A. McCarthy <sup>e,f,g</sup>

<sup>a</sup> Center for Composite Materials, University of Delaware, Newark, DE 19716, USA

<sup>b</sup> Department of Materials Science and Engineering, University of Delaware, Newark, DE 19716, USA

<sup>c</sup> Department of Civil and Structural Engineering, University of Delaware, Newark, DE 19716, USA

<sup>d</sup> Department of Engineering Science and Mechanics, Virginia Polytechnic Institute and State University, Blacksburg, VA 24061, USA

<sup>e</sup> Composites Research Centre, University of Limerick, Ireland

<sup>f</sup> Materials and Surface Science Institute, University of Limerick, Ireland

<sup>g</sup> Department of Mechanical and Aeronautical Engineering, University of Limerick, Ireland

Received 2 November 2006; accepted 23 December 2006

Available online 25 January 2007

## Abstract

The meshless local Petrov–Galerkin (MLPG) method with radial basis functions (RBFs), and the higher order shear and normal deformable plate theory (HOSNDPT) are used to analyze static infinitesimal deformations of thick laminated composite elastic plates under different boundary conditions. Two types of RBFs, namely, multiquadrics (MQ) and thin plate splines (TPS), are employed for constructing trial functions while a fourth order spline function is used as the test function. Computed results for different lamination schemes are found to match well with those obtained by other researchers. A benefit of using RBFs over those generated by the moving least squares approximation is that no special treatment is needed to impose essential boundary conditions, which substantially reduces the computational cost. Furthermore, the MLPG method does not require nodal connectivity which reduces the time required to prepare the input data.

© 2007 Elsevier Ltd. All rights reserved.

**Keywords:** A. Laminates; A. Plates; B. Elasticity; C. Numerical analysis

## 1. Introduction

Composite structures are widely used in the aerospace, automotive and marine industries, and a number of plate theories have been developed to analyze deformations of composite plates. The classical Kirchhoff thin plate theory (CLT), which ignores transverse shear effects, provides reasonable results for thin plates. However, it may not give accurate results for moderately thick plates. An improvement on the CLT is the first-order shear deformation the-

ory (FSDT) such as the Reissner–Mindlin theory which accounts for transverse shear effects, but needs a shear correction factor. Second- and higher-order shear deformation plate theories [1–4] use higher-order polynomials in the expansion of displacement components through the plate thickness and do not require shear correction factors. Among them, the higher-order shear and normal deformable plate theory (HONSNDPT) [3,5] accounts for both the transverse normal and the transverse shear deformations and uses Legendre polynomials as basis functions. Salient features of the theory include the satisfaction of natural boundary conditions prescribed on the top and the bottom surfaces of the plate, and computations of the transverse normal and the transverse shear stresses from the plate

\* Corresponding author. Tel.: +1 302 8316109; fax: +1 302 8318525.  
E-mail address: [xiaojr@udel.edu](mailto:xiaojr@udel.edu) (J.R. Xiao).

equations rather than by integration through the thickness of the balance of linear momentum. The HOSNDPT can accurately predict through-the-thickness modes of vibration, which correspond to null lateral displacements or deflections. The plate theory is called compatible if stresses are derived from the assumed displacement field and Hooke's Law, and mixed if stresses and displacements are expanded independently through the plate thickness. The mixed theory was originally developed for piezoelectric plates and has been used for studying free vibrations, and the propagation of plane waves in a thick anisotropic plate [5,6]. The compatible theory has been used for analyzing static and dynamic deformations of isotropic homogeneous [7] and functionally graded (FG) thick plates [8], and transient thermomechanical deformations of a FG plate [9]. Here we extend the HOSNDPT to analyze anisotropic thick composite laminate plates.

Meshless methods have recently attracted increasing attention in the computational community for finding approximate solutions of initial-boundary-value and boundary-value problems governed by partial differential equations. These include the element-free Galerkin (EFG) method [10], the reproducing kernel particle method (RKPM) [11], hp-clouds [12], and the Partition of Unity method (PUM) [13] which use a background mesh to numerically evaluate integrals appearing in the global weak formulation of the problem. The meshless local Petrov–Galerkin (MLPG) method [14–16] is based on a local weak formulation of the problem, and integrals appearing in it are evaluated without using a background mesh. Any non-element based interpolation scheme such as the moving least squares (MLS), the PUM, the smoothed particle hydrodynamics [17], or the modified smoothed particle hydrodynamics [18] can be used to generate basis functions for the trial solution and, if desired, also for the test function. Different test functions in the MLPG method result in schemes labeled as MLPG1 to MLPG6 in [16]. The flexibility in choosing the size and the shape of the local sub-domain leads to convenient formulations for different problems [14–16,19,20]. The MLS basis functions [7,8] lack the Kronecker delta property. A special technique such as the penalty parameter method or the method of Lagrange multipliers or a suitable modification of the system of simultaneous algebraic equations is required to satisfy essential boundary conditions, which considerably increases the computational cost. Recently radial basis functions (RBFs) [21] have been used to solve partial differential equations [22–24] and also as basis functions in meshless methods [25–29]. The resulting shape functions possess the Kronecker delta property which allows the essential boundary conditions to be imposed easily as in the finite element method. Furthermore, when RBFs are used in a local (compactly supported) rather than in a global interpolation scheme, such as in the EFG [27] and the MLPG methods [28], the dense system matrices associated with the global interpolation scheme are avoided. The extended multiquadrics,  $g(r) = (r^2 + c^2)^\beta$ , and thin plate

splines (TPS) have been successfully employed in the MLPG method [24] for the solution of two-dimensional (2D) stress analysis problems where the TPS was modified to  $g(r) = r^\alpha \log r$  with  $\alpha$  taken as a shape parameter. Here  $r$  is the distance between two points, and  $c$  and  $\beta$  are constants. Several developments have taken place in the analysis of composite plates using meshless methods. Among these, Belinha and Dinis [30] and Peng et al. [31] have combined the EFG method and Wang et al. [32] the RKPM with the FSDT to analyze deformations of composite laminates. Ferreira et al. have successfully used global RBFs in the analysis of composite plates using the first- [33] and the third- [34] order shear deformation theories as well as a trigonometric layerwise deformation theory [35]. However, the HOSNDPT theory with meshless methods has not been used to analyze composite laminates. The HOSNDPT in conjunction with the MLPG method employing the MLS and the radial basis functions has been used to analyze various problems of thick isotropic homogeneous and FG plates [7,8,36–41].

Here the MLPG method using RBFs is combined with the compatible HOSNDPT to analyze static deformations of thick composite laminates. Two types of RBFs, MQ and TPS, are employed as trial functions while a fourth-order spline function is used as the test function. Details of their implementation are given. Numerical examples are presented to demonstrate the convergence and the efficiency of the developed method. Computed results for different orders of the HOSNDPT are compared with published results from other plate theories, 3D analytical solutions as well as results from the analysis of the 3D problem with the finite element method (FEM) using the commercial code ABAQUS, and excellent agreements are achieved.

## 2. Review of the compatible higher-order shear and normal deformable plate theory (HOSNDPT)

A rectangular Cartesian coordinate system, shown in Fig. 1, is used to describe infinitesimal deformations of a rectangular plate occupying the region  $\Omega$  defined by  $0 \leq x \leq a$ ,  $0 \leq y \leq b$ , and  $-t/2 \leq z \leq t/2$ . The mid-surface,  $z = 0$ , of the plate is denoted by  $S$ , and displacements of a point along the  $x$ -, the  $y$ -, and the  $z$ -axes by  $u$ ,  $v$ , and  $w$ , respectively. Displacements are expanded in the thickness ( $z$ ) direction in terms of the orthonormal Legendre polynomials satisfying

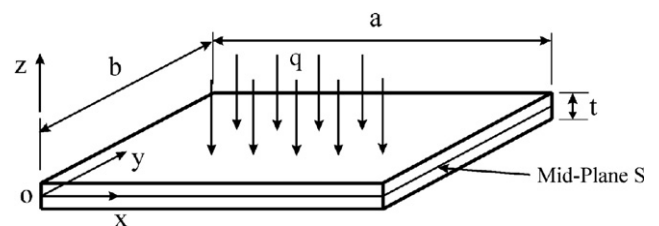


Fig. 1. A schematic sketch of the problem studied.

$$\int_{-t/2}^{t/2} L_i(z)L_j(z)dz = \delta_{ij}, i, j = 0, 1, 2, \dots, \tag{1}$$

where  $\delta_{ij}$  is the Kronecker delta, and  $L_i(z)$  is the  $i$ th Legendre polynomial. Orthonormal Legendre polynomials are equivalent to the basis  $1, z, z^2, \dots$ , and have the advantage of reducing the algebraic work. Expressions for the first seven orthonormal Legendre polynomials are:

$$L_0(z) = \frac{1}{\sqrt{t}}, \quad L_1(z) = 2\sqrt{\frac{3}{t}}z, \tag{2a}$$

$$L_2(z) = \frac{1}{2}\sqrt{\frac{5}{t}}\left[12\left(\frac{z}{t}\right)^2 - 1\right], \tag{2b}$$

$$L_3(z) = \sqrt{\frac{7}{t}}\left[-3\left(\frac{z}{t}\right) + 20\left(\frac{z}{t}\right)^3\right], \tag{2c}$$

$$L_4(z) = \frac{3}{\sqrt{t}}\left[\frac{3}{8} - 15\left(\frac{z}{t}\right)^2 + 70\left(\frac{z}{t}\right)^4\right], \tag{2d}$$

$$L_5(z) = \sqrt{\frac{11}{t}}\left[\frac{15}{4}\left(\frac{z}{t}\right) - 70\left(\frac{z}{t}\right)^3 + 252\left(\frac{z}{t}\right)^5\right], \tag{2e}$$

$$L_6(z) = \sqrt{\frac{13}{t}}\left[-\frac{5}{16} + \frac{105}{4}\left(\frac{z}{t}\right)^2 - 315\left(\frac{z}{t}\right)^4 + 924\left(\frac{z}{t}\right)^6\right], \tag{2f}$$

$$L_7(z) = \sqrt{\frac{15}{t}}\left[-\frac{35}{8}\left(\frac{z}{t}\right) + \frac{315}{2}\left(\frac{z}{t}\right)^3 - 1386\left(\frac{z}{t}\right)^5 + 3432\left(\frac{z}{t}\right)^7\right]. \tag{2g}$$

We set

$$\mathbf{u} = \begin{Bmatrix} u(x, y, z) \\ v(x, y, z) \\ w(x, y, z) \end{Bmatrix} = \sum_{i=0}^K \begin{Bmatrix} u_i(x, y) \\ v_i(x, y) \\ w_i(x, y) \end{Bmatrix} L_i(z), \tag{3}$$

where  $K$  is the order of the plate theory; for  $K \geq 2$ , the plate theory is called higher order. It should be noted that  $u_i, v_i, w_i$  ( $i = 0, 1, 2, \dots, K$ ) have units of (length)<sup>3/2</sup> since the dimension of an orthonormal Legendre polynomial is  $1/(\text{length})^{1/2}$ . Recalling that  $L'_i(z) = dL_i/dz$  is a polynomial of degree  $(i - 1)$  in  $z$ , we write

$$L'_i(z) = \sum_{j=0}^K d_{ij}L_j(z), \tag{4}$$

where  $d_{ij}$  are constants. For  $K = 7$ ,

$$d_{ij} = \begin{bmatrix} 0 & 0 & 0 & 0 & 0 & 0 & 0 & 0 \\ \sqrt{3} & 0 & 0 & 0 & 0 & 0 & 0 & 0 \\ 0 & \sqrt{15} & 0 & 0 & 0 & 0 & 0 & 0 \\ \sqrt{7} & 0 & \sqrt{35} & 0 & 0 & 0 & 0 & 0 \\ 0 & 3\sqrt{3} & 0 & 3\sqrt{7} & 0 & 0 & 0 & 0 \\ \sqrt{11} & 0 & \sqrt{55} & 0 & 3\sqrt{11} & 0 & 0 & 0 \\ 0 & \sqrt{39} & 0 & \sqrt{91} & 0 & \sqrt{143} & 0 & 0 \\ \sqrt{15} & 0 & 5\sqrt{3} & 0 & 3\sqrt{15} & 0 & \sqrt{195} & 0 \end{bmatrix}. \tag{5}$$

Note that elements in the first row and the last column of the  $(K + 1) \times (K + 1)$  matrix  $d_{ij}$  are zeros. For infinitesimal deformations, the strains tensor  $\epsilon$  is given by

$$\epsilon = \begin{Bmatrix} \epsilon_{xx} \\ \epsilon_{yy} \\ \epsilon_{zz} \\ 2\epsilon_{yz} \\ 2\epsilon_{zx} \\ 2\epsilon_{xy} \end{Bmatrix} = \sum_{i=0}^K \begin{Bmatrix} \frac{\partial u_i(x,y)}{\partial x} \\ \frac{\partial v_i(x,y)}{\partial y} \\ \sum_{j=0}^K w_j(x,y)d_{ji} \\ \frac{\partial w_i(x,y)}{\partial y} + \sum_{j=0}^K v_j(x,y)d_{ji} \\ \frac{\partial w_i(x,y)}{\partial x} + \sum_{j=0}^K u_j(x,y)d_{ji} \\ \frac{\partial v_i(x,y)}{\partial x} + \frac{\partial u_i(x,y)}{\partial y} \end{Bmatrix} L_i(z) \tag{6}$$

$$\equiv \sum_{i=0}^K \{\eta_i\} L_i(z),$$

where for  $i = 0, 1, 2, \dots, K$ ,  $\eta_i$  is a 6D vector with components

$$\eta_{i(1)} = \partial u_i / \partial x, \eta_{i(2)} = \partial v_i / \partial y, \eta_{i(3)} = \sum_{j=0}^K d_{ji} w_j, \tag{7a}$$

$$\eta_{i(4)} = \partial w_i / \partial y + \sum_{j=0}^K v_j d_{ji}, \eta_{i(5)} = \partial w_i / \partial x + \sum_{j=0}^K u_j d_{ji}, \tag{7b}$$

$$\eta_{i(6)} = \partial v_i / \partial x + \partial u_i / \partial y. \tag{7c}$$

The terms involving  $d_{ij}$  couple  $K$ th order displacements with those of lower order. Using Hooke's law, stresses at a material point  $\mathbf{x} = (x, y, z)$  are given by

$$\sigma = \{\sigma_{xx} \quad \sigma_{yy} \quad \sigma_{zz} \quad \sigma_{yz} \quad \sigma_{zx} \quad \sigma_{xy}\}^T = \mathbf{D}\epsilon \tag{8}$$

where  $\mathbf{D}$  is the matrix of elastic constants. Substitution from Eqs. (6) and (7) into Eq. (8) gives stresses at a point  $(x, y, z)$  in terms of displacements and in-plane gradients of displacements at the point  $(x, y, 0)$ .

### 3. Constitutive relations for a lamina

For an orthotropic material such as a unidirectional composite lamina, stresses at a material point in local rectangular Cartesian coordinate axes with the  $x$ -axis along the fiber are given by

$$\begin{Bmatrix} \sigma_{11} \\ \sigma_{22} \\ \sigma_{33} \\ \sigma_{23} \\ \sigma_{13} \\ \sigma_{12} \end{Bmatrix} = \begin{bmatrix} C_{11} & C_{12} & C_{13} & 0 & 0 & 0 \\ C_{21} & C_{22} & C_{23} & 0 & 0 & 0 \\ C_{31} & C_{32} & C_{33} & 0 & 0 & 0 \\ 0 & 0 & 0 & C_{44} & 0 & 0 \\ 0 & 0 & 0 & 0 & C_{55} & 0 \\ 0 & 0 & 0 & 0 & 0 & C_{66} \end{bmatrix} \begin{Bmatrix} \epsilon_{11} \\ \epsilon_{22} \\ \epsilon_{33} \\ 2\epsilon_{23} \\ 2\epsilon_{13} \\ 2\epsilon_{12} \end{Bmatrix}, \tag{9}$$

where subscripts 1 and 2 are the fiber and the in-plane normal to the fiber directions and 3 is the direction normal to

the plate. In terms of the more familiar parameters of an elastic material, the elastic constants  $C_{ij}$  are given by

$$C_{11} = \frac{1 - \nu_{23}\nu_{32}}{E_2E_3\Delta}, \quad C_{12} = \frac{\nu_{21} + \nu_{31}\nu_{23}}{E_2E_3\Delta}, \quad (10a)$$

$$C_{13} = \frac{\nu_{31} + \nu_{21}\nu_{32}}{E_2E_3\Delta}, \quad C_{22} = \frac{1 - \nu_{13}\nu_{31}}{E_1E_3\Delta}, \quad (10b)$$

$$C_{23} = \frac{\nu_{32} + \nu_{12}\nu_{31}}{E_1E_3\Delta}, \quad C_{33} = \frac{1 - \nu_{12}\nu_{21}}{E_1E_2\Delta}, \quad (10c)$$

$$C_{44} = G_{23}, \quad C_{55} = G_{31}, \quad C_{66} = G_{12} \quad (10d)$$

where:

$$\Delta = \frac{1 - \nu_{12}\nu_{21} - \nu_{23}\nu_{32} - \nu_{31}\nu_{13} - 2\nu_{21}\nu_{32}\nu_{13}}{E_1E_2E_3} \quad (10e)$$

Using an in-plane coordinate transformation, the stress-strain relations in the global  $xyz$ -coordinate system can be written as

$$\begin{Bmatrix} \sigma_{xx} \\ \sigma_{yy} \\ \sigma_{zz} \\ \sigma_{xy} \\ \sigma_{xz} \\ \sigma_{yz} \end{Bmatrix} = \begin{bmatrix} \bar{C}_{11} & \bar{C}_{12} & \bar{C}_{13} & 0 & 0 & \bar{C}_{16} \\ \bar{C}_{12} & \bar{C}_{22} & \bar{C}_{23} & 0 & 0 & \bar{C}_{26} \\ \bar{C}_{13} & \bar{C}_{23} & \bar{C}_{33} & 0 & 0 & \bar{C}_{36} \\ 0 & 0 & 0 & \bar{C}_{44} & \bar{C}_{45} & 0 \\ 0 & 0 & 0 & \bar{C}_{45} & \bar{C}_{55} & 0 \\ \bar{C}_{16} & \bar{C}_{26} & \bar{C}_{36} & 0 & 0 & \bar{C}_{66} \end{bmatrix} \begin{Bmatrix} \varepsilon_{xx} \\ \varepsilon_{yy} \\ \varepsilon_{zz} \\ 2\varepsilon_{xy} \\ 2\varepsilon_{xz} \\ 2\varepsilon_{yz} \end{Bmatrix} \quad (11a)$$

where

$$\begin{aligned} \bar{C}_{11} &= C_{11}\cos^4\theta + 2(C_{12} + 2C_{66})\cos^2\theta\sin^2\theta + C_{22}\sin^4\theta \\ \bar{C}_{12} &= C_{12}\cos^4\theta + (C_{11} + C_{22} - 4C_{66})\cos^2\theta\sin^2\theta + C_{12}\sin^4\theta \\ \bar{C}_{13} &= C_{13}\cos^2\theta + C_{23}\sin^2\theta \\ \bar{C}_{16} &= (C_{11} - C_{12} - 2C_{66})\cos^3\theta\sin\theta + (2C_{66} + C_{12} - C_{22})\cos\theta\sin^3\theta \\ \bar{C}_{26} &= (C_{12} - C_{22} + 2C_{66})\cos^3\theta\sin\theta + (C_{11} - C_{12} - 2C_{66})\cos\theta\sin^3\theta \\ \bar{C}_{36} &= (C_{13} - C_{23})\cos\theta\sin\theta \\ \bar{C}_{22} &= C_{22}\cos^4\theta + 2(C_{12} + 2C_{66})\cos^2\theta\sin^2\theta + C_{11}\sin^4\theta \\ \bar{C}_{23} &= C_{23}\cos^2\theta + C_{13}\sin^2\theta \\ \bar{C}_{33} &= C_{33} \\ \bar{C}_{44} &= C_{44}\cos^2\theta + C_{55}\sin^2\theta \\ \bar{C}_{45} &= (C_{55} - C_{44})\cos\theta\sin\theta \\ \bar{C}_{55} &= C_{55}\cos^2\theta + C_{44}\sin^2\theta \\ \bar{C}_{66} &= (C_{11} + C_{22} - 2C_{12} - 2C_{66})\cos^2\theta\sin^2\theta + C_{66}(\cos^4\theta + \sin^4\theta) \end{aligned} \quad (11b)$$

in which  $\theta$  is the angle between the global  $x$ -axis and the local  $x$ -axis of each lamina.

#### 4. Compatibility conditions at an interface

Assuming that the layers of the composite are perfectly bonded together surface tractions and displacements should be continuous across an interface between two adjoining layers. Our assumption of the displacement field given by Eq. (3) ensures the continuity of displacements

across an interface. However, since the displacement field Eq. (3) is also continuously differentiable, stresses derived from it will not satisfy the continuity of surface tractions because properties of the materials of the adjoining layers are different. A possibility is to assume a displacement field like that given by Eq. (3) in each layer and use either the method of Lagrange multipliers or a penalty method to enforce the continuity of displacements and surface tractions. The method of Lagrange multipliers introduces numerous additional unknowns, and the penalty method may make the system of equations ill-conditioned. Several researchers have either employed such techniques or have used zig-zag plate theories, e.g. see Kapuria et al. [42–44]. However, as shown below in Fig. 7, the present approach gives very good results for laminated plates when the material properties of different layers are not drastically different such as having one layer comprised of a rubber-like material and the other of graphite/epoxy composite.

#### 5. Weak formulation of the problem

Let  $\tilde{u}, \tilde{v}$ , and  $\tilde{w}$  be three linearly independent functions defined on the mid-surface  $S$ . Multiplying equations expressing the balance of linear momentum in the  $x$ -, the  $y$ - and the  $z$ -directions by  $\tilde{u}, \tilde{v}$ , and  $\tilde{w}$ , respectively, adding the resulting equations, integrating the result over  $\Omega$ , and using the divergence theorem, we obtain the following weak form of the problem:

$$\begin{aligned} \int_{\Omega} \tilde{\varepsilon}^T \sigma d\Omega - \int_{\Gamma_u} \tilde{\mathbf{u}}^T \sigma \mathbf{n} d\Gamma - \int_{\Omega} \tilde{\mathbf{u}}^T \mathbf{f} d\Omega - \int_{\Gamma_r} \tilde{\mathbf{u}}^T \bar{\mathbf{f}} d\Gamma \\ - \int_S \tilde{\mathbf{u}}^T q^{\pm} dS = 0. \end{aligned} \quad (12)$$

Here  $\mathbf{n}$  is the unit outward normal on the boundary  $\partial\Omega$ ,  $\mathbf{f}$  is the body force vector,  $\tilde{\varepsilon}$  is the strain vector obtained from Eq. (6) with  $u, v$ , and  $w$  replaced by  $\tilde{u}, \tilde{v}$ , and  $\tilde{w}$ , respectively,  $\{q^{\pm}\}$  is the traction on the top and the bottom surfaces of the plate,  $\Gamma_u$  and  $\Gamma_r$  are disjoint parts of the boundary  $\Gamma$  of  $S$  where displacements and surface tractions are prescribed, respectively, as  $\bar{u}$  and  $\bar{f}$ . Neglecting the body force, substituting from Eqs. (6), (8) and (11) into Eq. (12), and integrating with respect to  $z$  from  $-t/2$  to  $t/2$  gives

$$\begin{aligned} \sum_{i=0}^K \sum_{j=0}^K \left[ \int_S \{\tilde{\eta}_i\}^T [D_{ij}] \{\eta_j\} dS - \int_{\Gamma_u} \{\tilde{\eta}_i\}^T [n] [D_{ij}] \{\eta_j\} dS \right] \\ = \sum_{i=0}^K \left[ \int_{\Gamma_r} \{\tilde{u}\}_i^T \{\bar{f}_i\} d\Gamma + L_i \left( \pm \frac{t}{2} \right) \int_S \{\tilde{u}_i\}^T \{q^{\pm}\} dS \right] \end{aligned} \quad (13)$$

where

$$\{\bar{f}_i\} = \int_{-t/2}^{t/2} L_i(z) \{f\} dz. \quad (14)$$

The matrix  $[D_{ij}]$  of elastic constants has size  $6(K+1) \times 6(K+1)$  and is obtained by using the following relation

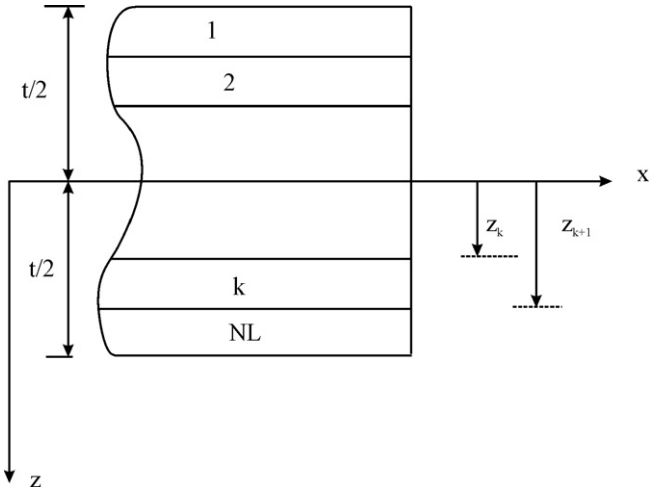


Fig. 2. Layer order and co-ordinate system.

$$[D_{ij}] = \int_{-t/2}^{t/2} [D]L_i(z)L_j(z)dz = \sum_{k=1}^{NL} \int_{z_k}^{z_{k+1}} [D]L_i(z)L_j(z)dz \quad (15)$$

where  $NL$  is the total number of layers in the laminate, shown in Fig. 2, and  $z_k$  and  $z_{k+1}$  are the  $z$ -co-ordinates of a point in the bottom and in the top surfaces of the  $k$ th layer. The matrix  $[D]$  is obtained using Eqs. (9–11). For a plate made of a homogeneous material, Eq. (15) simplifies to  $[D_{ij}] = [D]\delta_{ij}$ .

## 6. Radial basis functions and implementation of the MLPG method

### 6.1. Interpolation using radial basis functions

Consider a continuous function  $u(\mathbf{x})$  defined on the domain  $S$  having suitably located nodes. Using polynomial and RBFs, an interpolation Eq. (16) of  $u(\mathbf{x})$  in terms of quantities evaluated at nodes surrounding a point  $\mathbf{x}_Q$  can be written as

$$u(\mathbf{x}, \mathbf{x}_Q) = \sum_{i=1}^n g_i(\mathbf{x})a_i(\mathbf{x}_Q) + \sum_{j=1}^m p_j(\mathbf{x})b_j(\mathbf{x}_Q), \quad (16)$$

$$\sum_{i=1}^n p_j(x_i, y_i)a_i = 0, \quad j = 1, 2, \dots, m, \quad (17)$$

where  $n$  is the number of nodes in the neighborhood of  $\mathbf{x}_Q$ ,  $g_i(\mathbf{x})$  is a RBF,  $p_j(\mathbf{x})$  a monomial,  $m \ll n$  the number of monomial terms, and constants  $a_i(\mathbf{x}_Q)$  and  $b_j(\mathbf{x}_Q)$  are coefficients to be determined.

Enforcing the interpolation to pass through the  $n$  nodes leads to the following system of simultaneous equations for the determination of  $a_i(\mathbf{x}_Q)$  and  $b_j(\mathbf{x}_Q)$ :

$$A \begin{Bmatrix} a \\ b \end{Bmatrix} = \begin{bmatrix} G_0 & P_0 \\ P_0^T & 0 \end{bmatrix} \begin{Bmatrix} a \\ b \end{Bmatrix} = \begin{Bmatrix} u^e \\ 0 \end{Bmatrix}, \quad (18)$$

where

$$u^e = [u_1, u_2, u_3, \dots, u_n]^T, \quad (19)$$

$$G_0 = \begin{bmatrix} g_1(x_1, y_1) & g_2(x_1, y_1) & \cdots & g_n(x_1, y_1) \\ g_1(x_2, y_2) & g_2(x_2, y_2) & \cdots & g_n(x_2, y_2) \\ \vdots & \vdots & \ddots & \vdots \\ g_1(x_n, y_n) & g_2(x_n, y_n) & \cdots & g_n(x_n, y_n) \end{bmatrix}_{n \times n}, \quad (20)$$

$$P_0 = \begin{bmatrix} p_1(x_1, y_1) & p_2(x_1, y_1) & \cdots & p_m(x_1, y_1) \\ p_1(x_2, y_2) & p_2(x_2, y_2) & \cdots & p_m(x_2, y_2) \\ \vdots & \vdots & \ddots & \vdots \\ p_1(x_n, y_n) & p_2(x_n, y_n) & \cdots & p_m(x_n, y_n) \end{bmatrix}_{n \times m}. \quad (21)$$

The interpolation of the function  $u(\mathbf{x})$  can then be expressed as

$$u(\mathbf{x}) = [G^T(\mathbf{x})P^T(\mathbf{x})]A^{-1} \begin{Bmatrix} u^e \\ 0 \end{Bmatrix} = \Phi(\mathbf{x})u^e, \quad (22)$$

where the shape function  $\Phi(\mathbf{x})$  is given by

$$\Phi(\mathbf{x}) = [\phi_1(\mathbf{x}), \phi_2(\mathbf{x}), \phi_3(\mathbf{x}), \dots, \phi_k(\mathbf{x}), \dots, \phi_n(\mathbf{x})], \quad (23)$$

with

$$\phi_k(\mathbf{x}) = \sum_{i=1}^n g_i(\mathbf{x})\bar{A}_{i,k} + \sum_{j=1}^m p_j(\mathbf{x})\bar{A}_{n+j,k}. \quad (24)$$

Here  $\bar{A}_{i,k}$  is the  $(i, k)$  element of the matrix  $A^{-1}$ . The derivatives of  $\phi_k(\mathbf{x})$  have the following expressions:

$$\frac{\partial \phi_k}{\partial x} = \sum_{i=1}^n \frac{\partial g_i}{\partial x} \bar{A}_{i,k} + \sum_{j=1}^m \frac{\partial p_j}{\partial x} \bar{A}_{n+j,k}, \quad (25)$$

$$\frac{\partial \phi_k}{\partial y} = \sum_{i=1}^n \frac{\partial g_i}{\partial y} \bar{A}_{i,k} + \sum_{j=1}^m \frac{\partial p_j}{\partial y} \bar{A}_{n+j,k}. \quad (26)$$

Among the many choices for RBFs we use the following multiquadrics (MQ) and the thin plate splines (TPS).

$$g_i(x, y) = (r_i^2 + c^2)^\beta, \quad (MQ) \quad (27)$$

$$g_i(x, y) = (r_i)^\alpha \log r_i, \quad (TPS). \quad (28)$$

Here, constants  $\beta$ ,  $c$  and  $\alpha$  are shape parameters, and  $r_i = [(x - x_i)^2 + (y - y_i)^2]^{1/2}$ .

### 6.2. Test function used in the MLPG1

In the MLPG1 method employed here, we use the following 4th order spline function as the weight function.

$$\psi_J = W(\mathbf{x} - \mathbf{x}_J) = \begin{cases} 1 - 6\left(\frac{d_J}{r_s}\right)^2 + 8\left(\frac{d_J}{r_s}\right)^3 - 3\left(\frac{d_J}{r_s}\right)^4, & 0 \leq d_J \leq r_s \\ 0, & d_J \geq r_s. \end{cases} \quad (29)$$

Here  $d_J = |\mathbf{x} - \mathbf{x}_J|$ , and  $r_s$  equals the support of the function  $W$ . We use circular subdomains  $\Omega$  of radius  $r_s$  centered

at the node located at  $x_i$ , hereafter also called node  $i$  or  $x_i$ ; thus the support of  $W$  equals the size of the subdomain.

### 6.3. Derivation of algebraic equations

Let  $S_i \subset S$  be a smooth 2D region associated with a node in  $S$ ,  $\Gamma_{ui} = \partial S_i \cap \Gamma_u$ ,  $\Gamma_{fi} = \partial S_i \cap \Gamma_f$  and  $\Gamma_{i0} = \partial S_i - \Gamma_{ui} - \Gamma_{fi}$ . Let  $\phi_1, \phi_2, \dots, \phi_N$ , and  $\psi_1, \psi_2, \dots, \psi_N$  be linearly independent functions defined on  $S_i$ . For a  $K$ th order plate theory there are  $3(K+1)$  unknowns at a point in  $S_i$  or  $S$ . We write these as a  $3(K+1)$ D array and set

$$\{u(x, y)\} = \sum_{J=1}^N [\phi_J(x, y)] \{\delta_J\}, \quad (30)$$

$$\{\tilde{u}(x, y)\} = \sum_{J=1}^N [\psi_J(x, y)] \{\tilde{\delta}_J\}, \quad (31)$$

where for each  $J$ ,  $\{\delta_J\}$  is a  $3(K+1)$ D array, and  $[\phi_J]$  a square matrix of  $3(K+1)$  rows and columns. Similarly,  $\{\tilde{\delta}_J\}$  is a  $3(K+1)$ D array, and  $[\psi_J]$  a square matrix of  $3(K+1)$  rows and columns. The shape functions  $\phi_J$  are obtained using the RBFs described above, and functions  $\psi_J$  equal the weight functions. The unknowns  $\{\delta_J\}$  are nodal displacements (similar to those in the FEM). Substitution from Eqs. (30) and (31) into Eq. (7) gives

$$\{\eta\} = \sum_{J=1}^N [B_J] \{\delta_J\}, \quad \{\tilde{\eta}\} = \sum_{J=1}^N [\tilde{B}_J] \{\tilde{\delta}_J\}, \quad (32)$$

where  $\{\eta\}$  is a  $6(K+1)$ D array, and  $B_J$  a  $6(K+1) \times 3(K+1)$  matrix. The  $6(K+1)$  rows of  $B_J$  can be divided into  $(K+1)$  blocks of 6 rows each. The six rows of the  $i$ th block of  $B_J$  are given below.

$$\begin{bmatrix} \overbrace{0 \quad 0 \quad 0}^0 & \overbrace{\partial \phi_J / \partial x \quad 0 \quad 0}^i & \overbrace{0 \quad 0 \quad 0}^K \\ 0 \quad 0 \quad 0 & 0 \quad \partial \phi_J / \partial y \quad 0 & 0 \quad 0 \quad 0 \\ 0 \quad 0 \quad \phi_J d_{0i} & 0 \quad 0 \quad \phi_J d_{ii} & 0 \quad 0 \quad \phi_J d_{Ki} \\ 0 \quad \phi_J d_{0i} & 0 & \phi_J d_{ii} \quad \partial \phi_J / \partial y & 0 \quad \phi_J d_{Ki} & 0 \\ \phi_J d_{0i} & 0 \quad 0 & \phi_J d_{ii} & 0 \quad \partial \phi_J / \partial x & \phi_J d_{Ki} & 0 \quad 0 \\ 0 \quad 0 \quad 0 & \partial \phi_J / \partial y \quad \partial \phi_J / \partial x & 0 & 0 & 0 & 0 \end{bmatrix} \quad (33)$$

Elements of matrix  $\tilde{B}_J$  are obtained from those of matrix  $B_J$  by replacing  $\phi_J$  with  $\psi_J$ . Replacing the domain  $S$  of integration in Eq. (12) by  $S_i$ , substituting for  $\{u\}$  and  $\{\tilde{u}\}$  from Eqs. (30) and (31), and requiring that the resulting equation hold for all choices of  $\{\tilde{\delta}\}$ , we arrive at the following system of algebraic equations:

$$[K_{IJ}] \{\delta_J\} = \{F_I\}, \quad (34)$$

where

$$\begin{aligned} [K_{IJ}] = & \int_{S_i} ([\tilde{B}_I]^T [D] [B_J]) d\Omega - \int_{\Gamma_{ui}} ([\psi_I]^T [n] [D] [B_J]) d\Gamma \\ & - \int_{\Gamma_{i0}} ([\psi_I]^T [n] [D] [B_J]) d\Gamma, \end{aligned} \quad (35)$$

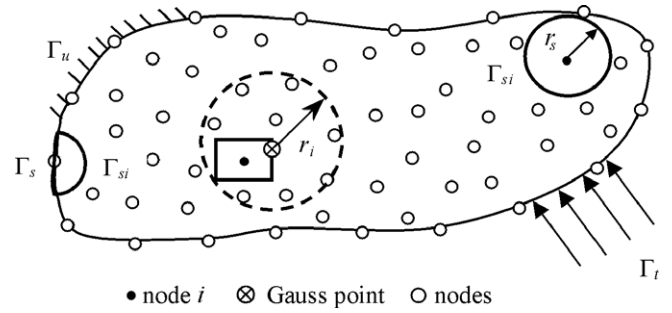


Fig. 3. The support and the interpolation domains used in deriving discrete equations for node  $i$ ; the region enclosed by a circle of radius  $r_s$  equals the support of node  $i$ , and that enclosed by the dotted circle of radius  $r_i$  represents the interpolation domain.

$$\{F_I\} = \int_{\Gamma_{fi}} [\psi_I]^T k \{\bar{f}\} d\Gamma + L_i(\pm t/2) \int_{S_i} [\psi_I]^T \{q^\pm\} d\Omega. \quad (36)$$

Equations similar to Eq. (34) are derived for each circular subdomain  $S_j$  with center at the node  $x_j$ . Gauss quadrature of an appropriate order is employed to numerically evaluate integrals over each subdomain. For each quadrature point, the trial solution is interpolated. Therefore, for a node  $x_i$  there are two local domains: the support of the test function which is a circle of radius  $r_s$  centered at  $x_i$ , and the interpolation domain of size  $r_i$  for each Gauss point. Fig. 3 shows the local subdomain for the node  $x_i$ , and the interpolation domain for the integration point  $x_Q$ . These two domains are independent of each other, and we set  $r_s = \alpha_s d_i$ , and  $r_i = \alpha_i d_i$ , where  $\alpha_s$  and  $\alpha_i$  are constants, and  $d_i$  is the distance from the node  $x_i$  to the node nearest to it.

## 7. Numerical solution of problems

A number of problems have been analyzed to demonstrate the accuracy and the convergence of the present method. Our previous work on thick isotropic and homogeneous plates [36] has indicated that optimum values of shape parameters for plate problems are the same as those for 2D elasticity problems [28]. It was also found in [29] that for the Multiquadric RBFs, there is a wide range of acceptable values of the shape parameter  $c$  which yield good results; optimum values of shape parameters are  $c = 6d$ ,  $\beta = 1.99$  for MQ, and  $\alpha = 4$  for TPS where  $d$  is the minimum distance between any two nodes. We have found that these values also work for laminated plates. In the examples discussed below the body force field is set to zero.

In the following figures and tables, the deflection  $w$ , the in-plane normal stresses  $\sigma_{xx}$  and  $\sigma_{yy}$ , the transverse normal stress  $\sigma_{zz}$  and the transverse shear stresses  $\tau_{xy}$ ,  $\tau_{xz}$  and  $\tau_{yz}$ , are non-dimensionalized as

$$\bar{w}(x = a/2, y = a/2, z = 0) = \frac{100 E_m t^3}{q a^4} w, \quad (37a)$$

$$\bar{\sigma}_{xx}(x = a/2, y = a/2) = \frac{t^2}{qa^2} \sigma_{xx},$$

$$\bar{\sigma}_{yy}(x = a/2, y = a/2) = \frac{t^2}{qa^2} \sigma_{yy} \quad (37b)$$

$$\bar{\sigma}_{zz}(x = a/2, y = a/2) = \frac{t}{qa} \sigma_{zz},$$

$$\bar{\tau}_{yz}(x = a/2, y = 0) = \frac{t}{qa} \tau_{yz} \quad (37c)$$

$$\bar{\tau}_{xy}(x = a, y = a) = \frac{t^2}{qa^2} \tau_{xy},$$

$$\bar{\tau}_{xz}(x = 0, y = a/2) = \frac{10t}{qa} \tau_{xz} \quad (37d)$$

where  $q$  is the magnitude of the normal traction applied on the top surface of the plate. The co-ordinates of points where deflections and stresses are calculated are shown in Eqs. (37).

In the local co-ordinate or the material principal axes, values assigned to different material parameters are

$$E_1 = 250 \text{ GPa}, E_2 = E_3 = 10 \text{ GPa}, \nu_{12} = \nu_{23} = \nu_{13}$$

$$= 0.25, G_{12} = G_{13} = 5 \text{ GPa}, G_{23} = 2 \text{ GPa}$$

### 7.1. Simply supported laminated composite plates under uniformly distributed load

Deformations of a simply supported square plate with length  $a = 20$  cm and thickness  $t$  subjected to a uniformly

distributed load  $q = 100 \text{ kN/m}^2$  are analyzed. Boundary conditions imposed at a simply supported edge are

$$\sigma_{xx} = 0, \quad w = v = 0 \text{ on } x = 0, a$$

$$\sigma_{yy} = 0, \quad u = w = 0 \text{ on } y = 0, a$$

We note that these boundary conditions were used by Pagano [47] to analyze the problem analytically. For this analysis, four different symmetric lamination schemes are considered with thickness-to-length ratios,  $t/a$ , of 0.05, 0.1 and 0.2. Except for the analysis of the convergence of results with an increase in the number of nodes, the midsurface of the plate is discretized with  $13 \times 13$  uniformly distributed nodes. The lamination schemes considered are: (1) an orthotropic lamina of  $0^\circ$  orientation; (2) a 3-layer  $0^\circ/90^\circ/0^\circ$  laminate; (3) a 4-layer  $0^\circ/90^\circ/90^\circ/0^\circ$  laminate, and (4) a 5-layer  $0^\circ/90^\circ/90^\circ/90^\circ/0^\circ$  laminate. Thus the geometry and material properties of the plate are symmetric about its midsurface, but the loading is asymmetric since only the top surface of the plate is loaded.

#### 7.1.1. Orthotropic lamina

The MQ and the TPS MLPG solutions are presented in Table 1 for  $K = 1, 3$  and 5 in the HOSNDPT, and are compared with results derived from the analytical solution obtained with the FSDT theory [45], the EFG solution with the FSDT [30], and the analysis of the 3D problem with the FEM using the commercial code ABAQUS and 20-noded brick elements. The number of uniform finite elements in the  $x$ - and the  $y$ -directions was increased from 10 to 40,

Table 1  
MQ and TPS MLPG1 solutions for different orders of the HOSNDPT (single orthotropic lamina and uniformly distributed load on the top surface)

$t/a$	Method	$\bar{w}$	$\bar{\sigma}_{xx}$	$\bar{\sigma}_{yy}$	$\bar{\tau}_{xy}$	$\bar{\tau}_{xz}$	$\bar{\tau}_{yz}$
0.05	3D-FEM	0.7255	0.7961	0.0277	0.05040	0.7674	0.1921
	FSDT-Exact [45]	0.7262	0.7828	0.0272	0.04870	0.6194	0.1466
	FSDT-EFG [30]	0.7281	0.7776	0.0285	0.04670	0.6041	0.1476
	MQ-MLPG1 ( $K = 1$ )	0.6988	0.7725	0.0310	0.04625	0.5200	0.1495
	MQ-MLPG1 ( $K = 3$ )	0.7169	0.7875	0.0278	0.04825	0.7600	0.2200
	MQ-MLPG1 ( $K = 5$ )	0.7169	0.7875	0.0275	0.04825	0.7550	0.2175
	TPS-MLPG1 ( $K = 1$ )	0.6919	0.7650	0.0310	0.04600	0.4760	0.1310
	TPS-MLPG1 ( $K = 3$ )	0.7094	0.7800	0.0275	0.04775	0.710	0.1945
	TPS-MLPG1 ( $K = 5$ )	0.7094	0.7800	0.0275	0.04775	0.705	0.1930
0.1	3D-FEM	0.9478	0.8227	0.0370	0.0616	0.7346	0.1914
	FSDT-Exact [45]	0.9519	0.7706	0.0352	0.0539	0.6147	0.1529
	FSDT-EFG [30]	0.9537	0.7655	0.0362	0.0523	0.5945	0.1463
	MQ-MLPG1 ( $K = 1$ )	0.8870	0.7640	0.0386	0.0513	0.5420	0.1530
	MQ-MLPG1 ( $K = 3$ )	0.9400	0.8160	0.0376	0.0558	0.7400	0.2030
	MQ-MLPG1 ( $K = 5$ )	0.9400	0.8160	0.0372	0.0558	0.7290	0.1950
	TPS-MLPG1 ( $K = 1$ )	0.8820	0.7600	0.0386	0.0514	0.5220	0.1430
	TPS-MLPG1 ( $K = 3$ )	0.9350	0.8120	0.0376	0.0557	0.7210	0.1910
	TPS-MLPG1 ( $K = 5$ )	0.9350	0.8120	0.0372	0.0557	0.7110	0.1880
0.2	3D-FEM	1.7783	0.9234	0.0667	0.1005	0.6595	0.2060
	MQ-MLPG1 ( $K = 1$ )	1.6056	0.7280	0.0620	0.0664	0.5880	0.1956
	MQ-MLPG1 ( $K = 3$ )	1.7696	0.9240	0.0688	0.0760	0.6760	0.2120
	MQ-MLPG1 ( $K = 5$ )	1.7696	0.9160	0.0672	0.0780	0.6560	0.2060
	TPS-MLPG1 ( $K = 1$ )	1.5992	0.7240	0.0620	0.0568	0.5700	0.1848
	TPS-MLPG1 ( $K = 3$ )	1.7624	0.9200	0.0688	0.0760	0.6660	0.2060
	TPS-MLPG1 ( $K = 5$ )	1.7624	0.9160	0.0672	0.0788	0.6460	0.1994

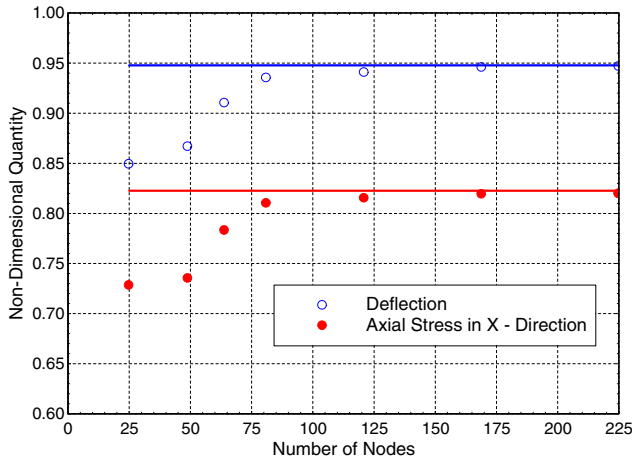


Fig. 4. Convergence of the centroidal deflection and the axial stress at the center of the plate’s top surface (MQ MLPG1) with an increase in the number of nodes (The solid lines represent the solution of the 3D problem by the FEM).

and in the  $z$ -direction from 5 to 24 until the solution converged. Results presented herein are based on the FE mesh with a quarter of the plate divided into 4800 elements having 20 elements each in the  $x$ - and the  $y$ -directions, and 12 elements in the thickness ( $z$ -) direction. While discussing these results, the solution obtained with ABAQUS is taken as the reference. For the MLPG1 method, the convergence with an increase in the number of uniformly placed nodes on each side of the plate has been studied by computing

results for seven different nodal densities, namely  $5 \times 5$ ,  $7 \times 7$ ,  $8 \times 8$ ,  $9 \times 9$ ,  $11 \times 11$ ,  $13 \times 13$  and  $15 \times 15$ . Values of other parameters were  $t/a = 0.1$ ,  $K = 5$ ,  $\alpha_s = 0.75$  and  $\alpha_i = 4$ . Results are plotted in Fig. 4 where solid lines represent the solution of the 3D problem computed with the FEM. It can be seen from Fig. 4 that both the centroidal deflection and the axial stress at the center of the top surface computed with the MLPG1 method converge with an increase in the number of nodes both for the MQ and the TPS basis functions. Converged results are obtained with 169 nodes.

In general, it can be seen from Table 1 that as the order of the plate theory is increased from 1 to 5, both the deflection and stresses at the selected points approach their respective values for the reference solution. Except for the transverse shear stresses, the FSDT gives good values of the stresses and the deflection for the thin plate with  $t/a = 0.05$ . For the moderately thick plate with  $t/a = 0.1$  the FSDT gives reasonable values of stresses and deflections. For the thick plate with  $t/a = 0.2$ , the present 5th order HOSNDPT gives results that are close to those obtained from the analysis of the 3D problem with ABAQUS. Both the TPS and the MQ basis functions perform equally well.

### 7.1.2. Laminated plates

For the  $0^\circ/90^\circ/0^\circ$ ,  $0^\circ/90^\circ/90^\circ/0^\circ$ , and the  $0^\circ/90^\circ/90^\circ/90^\circ/0^\circ$  laminates, we have listed in Tables 2–4 the centroidal deflection and the stresses at different points as computed

Table 2  
MQ and TPS MLPG1 solutions for different orders of the plate theory ( $0^\circ/90^\circ/0^\circ$  laminate, uniformly distributed load)

$t/a$	Method	$\bar{w}$	$\bar{\sigma}_{xx}$	$\bar{\sigma}_{yy}$	$\bar{\tau}_{xy}$	$\bar{\tau}_{xz}$	$\bar{\tau}_{yz}$
0.05	3D-FEM	0.7951	0.8247	0.2391	0.0493	0.690	0.3910
	FSDT-Exact [45]	0.7572	0.7983	0.2227	0.0453	0.770	0.2902
	FSDT-EFG [30]	0.7583	0.7905	0.2279	0.0441	0.744	0.2264
	MQ-MLPG1 ( $K = 1$ )	0.7256	0.7875	0.2175	0.0430	0.645	0.2760
	MQ-MLPG1 ( $K = 3$ )	0.7688	0.8125	0.2300	0.0458	1.070	0.3570
	MQ-MLPG1 ( $K = 5$ )	0.7688	0.8125	0.2300	0.0458	1.070	0.3570
	TPS-MLPG1 ( $K = 1$ )	0.7188	0.7800	0.2160	0.0425	0.590	0.2315
	TPS-MLPG1 ( $K = 3$ )	0.7613	0.8050	0.2285	0.0453	1.010	0.3025
	TPS-MLPG1 ( $K = 5$ )	0.7694	0.8050	0.2318	0.0453	1.095	0.3045
0.1	3D-FEM	1.1541	0.8709	0.3621	0.0661	0.630	0.4060
	FSDT-Exact [45]	1.0219	0.7719	0.3072	0.0514	0.755	0.3107
	FSDT-EFG [30]	1.0225	0.7646	0.3105	0.0500	0.725	0.2958
	MQ-MLPG1 ( $K = 1$ )	0.9465	0.7660	0.2900	0.0484	0.660	0.2850
	MQ-MLPG1 ( $K = 3$ )	1.0860	0.8530	0.3380	0.0561	1.030	0.3560
	MQ-MLPG1 ( $K = 5$ )	1.1115	0.8570	0.3490	0.0567	1.090	0.3550
	TPS-MLPG1 ( $K = 1$ )	0.9415	0.7630	0.2900	0.0484	0.637	0.2640
	TPS-MLPG1 ( $K = 3$ )	1.0800	0.8480	0.3370	0.0559	1.000	0.3320
	TPS-MLPG1 ( $K = 5$ )	1.1055	0.8520	0.3470	0.0565	1.070	0.3310
0.2	3D-FEM	2.3218	1.0215	0.6629	0.1140	0.595	0.4690
	MQ-MLPG1 ( $K = 1$ )	1.7572	0.7000	0.5000	0.0632	0.684	0.3520
	MQ-MLPG1 ( $K = 3$ )	2.1644	0.9960	0.6120	0.0856	0.892	0.4180
	MQ-MLPG1 ( $K = 5$ )	2.2136	0.9960	0.6280	0.0884	0.930	0.4360
	TPS-MLPG1 ( $K = 1$ )	1.7504	0.6960	0.5000	0.0636	0.666	0.3360
	TPS-MLPG1 ( $K = 3$ )	2.1556	0.9960	0.6080	0.0856	0.876	0.4020
	TPS-MLPG1 ( $K = 5$ )	2.2044	0.9960	0.6280	0.0888	0.912	0.4180

Table 3  
MQ and TPS MLPG1 solutions for different orders of the plate theory (0°/90°/90°/0° laminate, uniformly distributed load)

$t/a$	Method	$\bar{w}$	$\bar{\sigma}_{xx}$	$\bar{\sigma}_{yy}$	$\bar{\tau}_{xy}$	$\bar{\tau}_{xz}$	$\bar{\tau}_{yz}$
0.05	3D-FEM	0.8029	0.8228	0.4168	0.0457	0.622	0.4738
	FSDT-Exact [45]	0.7694	0.8045	0.3968	0.0420	0.831	0.3228
	FSDT-EFG [30]	0.7698	0.7948	0.3970	0.0414	0.796	0.3108
	MQ-MLPG1 ( $K = 1$ )	0.7369	0.7950	0.3850	0.0400	0.690	0.2845
	MQ-MLPG1 ( $K = 3$ )	0.7844	0.8125	0.4075	0.0428	1.000	0.3925
	MQ-MLPG1 ( $K = 5$ )	0.7881	0.8125	0.4100	0.0430	0.920	0.4425
	TPS-MLPG1 ( $K = 1$ )	0.7306	0.7875	0.3825	0.0395	0.640	0.2385
	TPS-MLPG1 ( $K = 3$ )	0.7775	0.8050	0.4050	0.0423	0.945	0.3390
TPS-MLPG1 ( $K = 5$ )	0.7819	0.8050	0.4075	0.0425	0.865	0.3875	
0.1	3D-FEM	1.1401	0.8280	0.5617	0.0603	0.554	0.498
	FSDT-Exact [45]	1.0250	0.7577	0.5006	0.047	0.798	0.350
	FSDT-EFG [30]	1.0248	0.7494	0.4988	0.0458	0.763	0.332
	MQ-MLPG1 ( $K = 1$ )	0.9520	0.7570	0.4750	0.0452	0.700	0.313
	MQ-MLPG1 ( $K = 3$ )	1.1090	0.8280	0.5480	0.0541	0.949	0.439
	MQ-MLPG1 ( $K = 5$ )	1.1180	0.8230	0.5500	0.0550	0.879	0.475
	TPS-MLPG1 ( $K = 1$ )	0.9465	0.7530	0.4730	0.0448	0.675	0.279
	TPS-MLPG1 ( $K = 3$ )	1.0955	0.8240	0.5410	0.0539	0.922	0.430
TPS-MLPG1 ( $K = 5$ )	1.1125	0.8200	0.5490	0.0544	0.852	0.466	
0.2	3D-FEM	2.2383	0.908	0.861	0.1072	0.568	0.4487
	MQ-MLPG1 ( $K = 1$ )	1.7208	0.664	0.696	0.0564	0.704	0.402
	MQ-MLPG1 ( $K = 3$ )	2.1496	0.904	0.820	0.0828	0.424	0.496
	MQ-MLPG1 ( $K = 5$ )	2.1828	0.896	0.828	0.0860	0.768	0.536
	TPS-MLPG1 ( $K = 1$ )	1.7136	0.660	0.684	0.0560	0.682	0.338
	TPS-MLPG1 ( $K = 3$ )	2.1400	0.900	0.816	0.0812	0.796	0.484
	TPS-MLPG1 ( $K = 5$ )	2.1728	0.892	0.824	0.0840	0.750	0.524

Table 4  
MQ and TPS MLPG1 solutions for varying orders of plate theory (0°/90°/90°/0° laminate, uniformly distributed load)

$t/a$	Method	$\bar{w}$	$\bar{\sigma}_{xx}$	$\bar{\sigma}_{yy}$	$\bar{\tau}_{xy}$	$\bar{\tau}_{xz}$	$\bar{\tau}_{yz}$
0.05	3D-FEM	0.7794	0.8207	0.4870	0.0444	0.6040	0.4545
	FSDT-Exact [45]	0.7581	0.8080	0.4844	0.0403	0.7166	0.4188
	FSDT-EFG [30]	0.7584	0.7980	0.4819	0.0399	0.6856	0.3995
	MQ-MLPG1 ( $K = 1$ )	0.7288	0.7975	0.4725	0.0385	0.6000	0.3610
	MQ-MLPG1 ( $K = 3$ )	0.7506	0.8100	0.4775	0.0405	0.9200	0.5650
	MQ-MLPG1 ( $K = 5$ )	0.7538	0.8100	0.4750	0.0408	0.8250	0.6950
	TPS-MLPG1 ( $K = 1$ )	0.7219	0.7900	0.4700	0.0383	0.5450	0.3115
	TPS-MLPG1 ( $K = 3$ )	0.7438	0.8025	0.4725	0.0400	0.8550	0.5000
TPS-MLPG1 ( $K = 5$ )	0.7469	0.8050	0.4700	0.0403	0.7650	0.6300	
0.1	3D-FEM	1.0576	0.8201	0.5605	0.0577	0.5781	0.441
	FSDT-Exact [45]	0.9727	0.7649	0.5525	0.0436	0.6901	0.441
	FSDT-EFG [30]	0.9722	0.7565	0.5490	0.0424	0.6586	0.417
	MQ-MLPG1 ( $K = 1$ )	0.9085	0.7620	0.5330	0.0419	0.6090	0.392
	MQ-MLPG1 ( $K = 3$ )	0.9730	0.8020	0.5380	0.0478	0.8790	0.573
	MQ-MLPG1 ( $K = 5$ )	0.9865	0.8090	0.5350	0.0487	0.7970	0.684
	TPS-MLPG1 ( $K = 1$ )	0.9040	0.7590	0.5310	0.042	0.5860	0.370
	TPS-MLPG1 ( $K = 3$ )	0.9675	0.7980	0.5360	0.0478	0.8550	0.549
TPS-MLPG1 ( $K = 5$ )	0.9815	0.8050	0.5300	0.0488	0.7740	0.659	
0.2	3D-FEM	2.1044	0.8995	0.7386	0.0991	0.534	0.424
	MQ-MLPG1 ( $K = 1$ )	1.5864	0.6840	0.6640	0.0448	0.594	0.474
	MQ-MLPG1 ( $K = 3$ )	1.8100	0.8400	0.6600	0.0696	0.778	0.600
	MQ-MLPG1 ( $K = 5$ )	1.8736	0.8640	0.6720	0.0740	0.732	0.686
	TPS-MLPG1 ( $K = 1$ )	1.5804	0.6840	0.6520	0.0492	0.610	0.454
	TPS-MLPG1 ( $K = 3$ )	1.8032	0.8360	0.6600	0.0700	0.766	0.586
	TPS-MLPG1 ( $K = 5$ )	1.8664	0.8640	0.6720	0.0748	0.716	0.670

with different plate theories and also with the 3D FEM (six uniform elements along the thickness of each layer). For

the thin plate, the FSDT gives good results for the centroidal deflection and the in-plane stresses. However, values of

transverse shear stresses computed with the FSDT show noticeable deviations from those computed with the FEM. As for the single lamina, the MQ and the TPS basis functions work equally well. For each laminate, the computed centroidal deflection and the in-plane stresses approach their analytical values as the order of the plate theory is increased from 1 to 5. However, the transverse shear stresses do not match well with those obtained from the analysis of the 3D problem. It is likely that their values computed by using the mixed HOSNDPT and/or satisfying the continuity of surface tractions across the interface between two adjoining layers will be considerably improved, but this has not been tried here. In general, stresses computed at plate edges are not as accurate as those at the center of the plate; similar trends were seen for isotropic homogeneous [36] and FG [37] plates. The difference in the two sets of results can possibly be reduced by using a dense distribution of nodes near the free edges. Note that a higher-order plate theory employs higher-order expansions of variables in the thickness coordinate and not within the plane of the midsurface of the plate. This is also true of the solution of the 3D elasticity equations by the finite element method. We add that results from the 3rd and the 5th order plate theories are quite close to each other implying that in most cases one can use the 3rd order shear and normal deformable plate theory.

In order to ascertain the order of the plate theory which gives converged results, the non-dimensional deflection and the axial stresses are plotted in Fig. 5 with the order of the HOSNDPT varying from 1 to 7 for the 0°/90°/90°/0° laminated plate and using MQ RBFs. It can be seen that  $K = 3$  in the HOSNDPT gives reasonably accurate results. Qian et al. [8] found that converged frequencies are obtained with  $K = 5$  in the HOSNDPT.

As mentioned previously, one of the advantages of the HOSNDPT is that the transverse normal and the transverse shear stresses are computed from equations of the

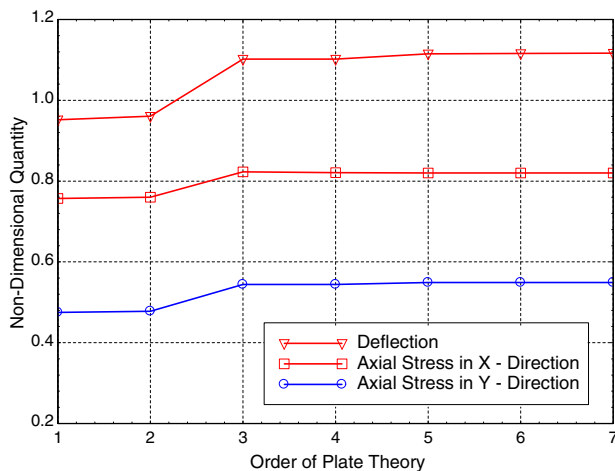


Fig. 5. Non-dimensional deflection  $\bar{w}$  and axial stresses  $\bar{\sigma}_{xx}$  and  $\bar{\sigma}_{yy}$  vs. order of plate theory  $K$  for a 0°/90°/90°/0° laminated plate using the MQ-MLPG1 method.

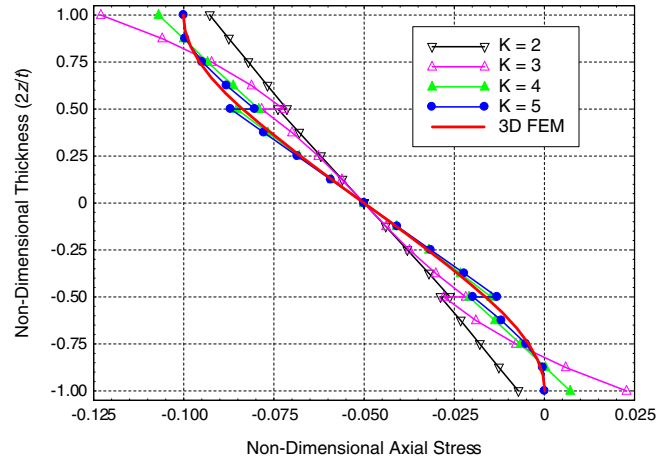


Fig. 6. Through-the-thickness distributions of the transverse normal stresses ( $\sigma_{zz}$ ) computed with the present method and the analysis of the 3D problem by the finite element method (0°/90°/90°/0° laminated plate).

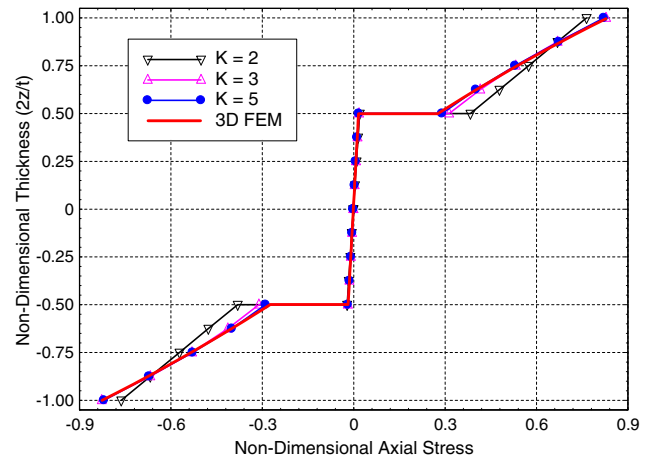


Fig. 7. Through-the-thickness variations of axial stress ( $\sigma_{xx}$ ) computed with the present method and the analysis of the 3D problem by the finite element method (0°/90°/90°/0° laminated plate).

plate theory. In order to see if  $\sigma_{zz}$  and  $\sigma_{xx}$  are accurately predicted, we plot in Figs. 6 and 7 their variations through the plate thickness for the 0°/90°/90°/0° laminate using the MQ RBFs and computed with values of  $K$  varying from 2 to 5. It is clear that as  $K$  increases from 2 to 5, the computed distributions of the transverse normal stress and the axial stress approach those obtained with the FEM which implies that the HOSNDPT with  $K = 5$  accurately predicts through-the-thickness distribution of the transverse normal stress, and jumps in the axial stress across interfaces between adjoining layers.

## 7.2. Laminated composite plates under sinusoidal loading

### 7.2.1. Simply supported laminated plates

Results are also computed for the 0°/90°/90°/0° laminate with tractions on the top surface given by  $q \sin(\pi x/a) \sin(\pi y/a)$  and are compared in Table 5 with the

Table 5  
MQ and TPS MLPG1 solutions for varying orders of plate theory ( $0^\circ/90^\circ/90^\circ/0^\circ$  laminate, sinusoidal load)

$t/a$	Method	$\bar{w}$	$\bar{\sigma}_{xx}$	$\bar{\sigma}_{yy}$	$\bar{\tau}_{xy}$	$\bar{\tau}_{xz}$	$\bar{\tau}_{yz}$
0.25	HSDT [46]	1.8937	0.6651	0.6322	0.0440	0.2064	–
	Elasticity [47]	1.9540	0.7200	0.6660	0.0467	0.2700	–
	Ferreira et al. [48]	1.8864	0.6659	0.6313	0.0430	0.1352	–
	MQ-MLPG1 ( $K = 1$ )	1.5016	0.4200	0.5506	0.0300	0.3175	0.1675
	MQ-MLPG1 ( $K = 3$ )	1.8703	0.7250	0.6169	0.0452	0.3825	0.2440
	MQ-MLPG1 ( $K = 5$ )	1.8930	0.7125	0.6313	0.0459	0.3575	0.2675
	TPS-MLPG1 ( $K = 1$ )	1.4984	0.4188	0.5500	0.0301	0.3125	0.1633
	TPS-MLPG1 ( $K = 3$ )	1.8672	0.7250	0.6163	0.0451	0.3775	0.2388
	TPS-MLPG1 ( $K = 5$ )	1.8898	0.7125	0.6250	0.0458	0.3525	0.2625
0.1	HSDT [46]	0.7147	0.5456	0.3888	0.0268	0.2640	–
	Elasticity [47]	0.7430	0.5590	0.4030	0.0276	0.3010	–
	Ferreira et al. [48]	0.5070	0.5405	0.3648	0.0228	0.3818	–
	MQ-MLPG1 ( $K = 1$ )	0.6170	0.5010	0.3460	0.0233	0.3460	0.103
	MQ-MLPG1 ( $K = 3$ )	0.7155	0.5580	0.3900	0.0269	0.4930	0.154
	MQ-MLPG1 ( $K = 5$ )	0.7245	0.5560	0.3940	0.0271	0.4500	0.175
	TPS-MLPG1 ( $K = 1$ )	0.6155	0.5000	0.3450	0.0233	0.3370	0.093
	TPS-MLPG1 ( $K = 3$ )	0.7135	0.5570	0.3890	0.0268	0.4800	0.141
	TPS-MLPG1 ( $K = 5$ )	0.7225	0.5550	0.3930	0.0270	0.4380	0.162
0.05	HSDT [46]	0.5061	0.5393	0.3043	0.0233	0.2825	–
	Elasticity [47]	0.5170	0.5430	0.3090	0.0230	0.3280	–
	Ferreira et al. [48]	0.4365	0.5413	0.3359	0.0215	0.4106	–
	MQ-MLPG1 ( $K = 1$ )	0.4724	0.5225	0.2875	0.0213	0.3500	0.0785
	MQ-MLPG1 ( $K = 3$ )	0.5036	0.5400	0.3025	0.0224	0.5200	0.1115
	MQ-MLPG1 ( $K = 5$ )	0.5063	0.5400	0.3050	0.0224	0.4735	0.1260
	TPS-MLPG1 ( $K = 1$ )	0.4700	0.5200	0.2875	0.0212	0.3180	0.0520
	TPS-MLPG1 ( $K = 3$ )	0.5009	0.5375	0.3025	0.0223	0.4825	0.0785
	TPS-MLPG1 ( $K = 5$ )	0.5036	0.5375	0.3025	0.0223	0.4370	0.0915

published results from the higher order plate theory of Reddy [44], the 3D elasticity solution of Pagano [47], and those computed by Ferreira et al. [48] with a meshless (collocation) method employing RBFs. For each one of the three laminates with  $t/a = 0.05, 0.1$  and  $0.25$ , the present values of the centroidal deflection  $\bar{w}$  and the axial stresses  $\bar{\sigma}_{xx}$  and  $\bar{\sigma}_{yy}$  are in excellent agreement with those obtained by other methods and in particular with Pagano's solution of the corresponding 3D elasticity problem. As pointed out earlier for plates subjected to a uniformly distributed load on the top surface, the transverse shear stresses at points on a plate's edge deviate somewhat from those given by the elasticity solution.

### 7.2.2. Laminated plates under other boundary conditions

Vel and Batra [49–51] have studied analytically deformations of thick laminated plates under general boundary conditions, and their analysis accounts for continuity conditions across interfaces and should give accurate results even when material properties of adjoining layers vary significantly. Eight different boundary conditions have been examined in [49] for the  $0^\circ/90^\circ$  and  $0^\circ/90^\circ/0^\circ$  laminates. Only the  $0^\circ/90^\circ$  laminate is analyzed here by using the present meshless method, and three boundary conditions (SSSS, SCSC and SFSF) are considered; here  $S$  = simply supported,  $C$  = clamped and  $F$  = free edge. The clamped and free boundary conditions are applied at the edges

$x = 0$  and  $x = a$  while the edges at  $y = 0$ , and  $y = a$  are held simply supported. Boundary conditions at the clamped and free edges are:

$$\text{Clamped: } u = v = w = 0, \text{ on } x = 0, a;$$

$$\text{Free: } \sigma_{xx} = \sigma_{xy} = \sigma_{xz} = 0, \text{ on } x = 0, a.$$

Results for the  $0^\circ/90^\circ$  laminate with  $t/a = 0.10$  and  $0.20$  and tractions on the top surface given by  $q \sin(\pi x/a) \sin(\pi y/a)$  are compared in Tables 6 and 7 with the published results from the 3D analytical solution of Vel and Batra [49], and the higher order plate theory of Khdeir and Reddy [52]. For each one of the three boundary conditions the present values of the centroidal deflection  $\bar{w}$  and the stresses  $\bar{\sigma}_{xx}$ ,  $\bar{\sigma}_{yy}$ ,  $\bar{\sigma}_{zz}$  and are in excellent agreement with those obtained by other methods and in particular with Vel and Batra's 3D analytical solution. It should be noted that different non-dimensionalization were used by Vel and Batra [49], and their results have been recalculated using Eqs. (37) for consistency. The transverse shear stress  $\bar{\tau}_{yz}$  at  $(x = a/2, y = 0)$  also agrees very well with that from the higher order plate theory [52] (not provided in Ref. [49]). The through-the-thickness distribution of the transverse shear stresses  $\bar{\tau}_{yz}$  at  $(x = 0.05a, y = 0)$  computed from the present method is compared with the analytical solution [49] in Fig. 8. The maximum shear stress at  $(x = 0.05a, y = 0)$  from the analytical solution is  $0.254q$ , and that from the present method equals  $0.222q, 0.235q$ ,

Table 6  
A square (0°/90°) laminate under different boundary conditions ( $t/a = 0.2$ , sinusoidal load)

BC	Method	$\bar{w}$	$\bar{\sigma}_{xx}$	$\bar{\sigma}_{yy}$	$\bar{\tau}_{zz}$	$\bar{\tau}_{xy}$	$\bar{\tau}_{yz}$
SSSS	3D Analytical [49]	1.712	-0.7671	0.7894	0.0990	0.0527	-
	HSDT [52]	1.667	-0.8385	0.8385	-	-	0.3155
	FSDT [52]	1.758	-0.7157	0.7157	-	-	0.2729
	MQ-MLPG1 ( $K = 1$ )	1.613	-0.7000	0.7120	0.0984	0.0476	0.2180
	MQ-MLPG1 ( $K = 3$ )	1.676	-0.7480	0.7720	0.0994	0.0516	0.2820
	MQ-MLPG1 ( $K = 5$ )	1.696	-0.7600	0.7840	0.1000	0.0524	0.3020
	TPS-MLPG1 ( $K = 1$ )	1.608	-0.6960	0.7080	0.0982	0.0476	0.2120
	TPS-MLPG1 ( $K = 3$ )	1.672	-0.7480	0.7680	0.0992	0.0516	0.2760
	TPS-MLPG1 ( $K = 5$ )	1.691	-0.7600	0.7800	0.0992	0.0524	0.2940
SCSC	3D Analytical [49]	1.217	-0.4630	0.5723	0.1158	0.0313	-
	HSDT [52]	1.088	-0.5679	0.5505	-	-	0.2095
	FSDT [52]	1.257	-0.3911	0.5153	-	-	0.1958
	MQ-MLPG1 ( $K = 1$ )	1.124	-0.3868	0.5000	0.1044	0.0271	0.1510
	MQ-MLPG1 ( $K = 3$ )	1.180	-0.4360	0.5560	0.1142	0.0298	0.2000
	MQ-MLPG1 ( $K = 5$ )	1.202	-0.4600	0.5680	0.1154	0.0311	0.2160
	TPS-MLPG1 ( $K = 1$ )	1.122	-0.3860	0.5000	0.1042	0.0268	0.1462
	TPS-MLPG1 ( $K = 3$ )	1.177	-0.4320	0.5520	0.1134	0.0295	0.1954
	TPS-MLPG1 ( $K = 5$ )	1.199	-0.4600	0.5640	0.1154	0.0307	0.2100
SFSF	3D Analytical [49]	2.753	-0.2660	1.2877	0.0718	0.0108	-
	HSDT [52]	2.624	-0.3171	1.3551	-	-	0.4457
	FSDT [52]	2.777	-0.2469	1.1907	-	-	0.3901
	MQ-MLPG1 ( $K = 1$ )	2.587	-0.2280	1.1880	0.0828	0.0104	0.3160
	MQ-MLPG1 ( $K = 3$ )	2.699	-0.2544	1.2560	0.0746	0.0105	0.4000
	MQ-MLPG1 ( $K = 5$ )	2.746	-0.2628	1.2880	0.0708	0.0106	0.4700
	TPS-MLPG1 ( $K = 1$ )	2.590	-0.2272	1.1920	0.0828	0.0104	0.3260
	TPS-MLPG1 ( $K = 3$ )	2.703	-0.2532	1.2560	0.0742	0.0105	0.4080
	TPS-MLPG1 ( $K = 5$ )	2.750	-0.2616	1.2880	0.0704	0.0106	0.4780

Table 7  
A square (0°/90°) laminate under different boundary conditions ( $t/a = 0.1$ , sinusoidal load)

BC	Method	$\bar{w}$	$\bar{\sigma}_{xx}$	$\bar{\sigma}_{yy}$	$\bar{\tau}_{zz}$	$\bar{\tau}_{xy}$	$\bar{\tau}_{yz}$
SSSS	3D Analytical [49]	1.227	-0.7304	0.7309	0.0500	0.0497	-
	HSDT [52]	1.216	-0.7468	0.7468	-	-	0.3190
	FSDT [52]	1.237	-0.7157	0.7157	-	-	0.2729
	MQ-MLPG1 ( $K = 1$ )	1.177	-0.7040	0.7040	0.0498	0.0471	0.2150
	MQ-MLPG1 ( $K = 3$ )	1.214	-0.7240	0.7250	0.0500	0.0491	0.2800
	MQ-MLPG1 ( $K = 5$ )	1.220	-0.7260	0.7270	0.0500	0.0494	0.2980
	TPS-MLPG1 ( $K = 1$ )	1.172	-0.7010	0.7010	0.0498	0.0469	0.1970
	TPS-MLPG1 ( $K = 3$ )	1.208	-0.7210	0.7220	0.0500	0.0488	0.2600
	TPS-MLPG1 ( $K = 5$ )	1.213	-0.7230	0.7240	0.0500	0.0491	0.2780
SCSC	3D Analytical [49]	0.649	-0.4653	0.3888	0.0640	0.0221	-
	HSDT [52]	0.617	-0.4952	0.3803	-	-	0.1725
	FSDT [52]	0.656	-0.4450	0.3799	-	-	0.1523
	MQ-MLPG1 ( $K = 1$ )	0.610	-0.4430	0.3650	0.1116	0.0203	0.1170
	MQ-MLPG1 ( $K = 3$ )	0.635	-0.4580	0.3820	0.0620	0.0214	0.1560
	MQ-MLPG1 ( $K = 5$ )	0.643	-0.4620	0.3850	0.0631	0.0219	0.1610
	TPS-MLPG1 ( $K = 1$ )	0.608	-0.4400	0.3640	0.0559	0.0200	0.1060
	TPS-MLPG1 ( $K = 3$ )	0.632	-0.4560	0.3800	0.0620	0.0211	0.1430
	TPS-MLPG1 ( $K = 5$ )	0.640	-0.4600	0.3840	0.0642	0.0215	0.1480
SFSF	3D Analytical [49]	2.026	-0.2503	1.2100	0.0360	0.0119	-
	HSDT [52]	2.624	-0.3171	1.3551	-	-	0.4489
	FSDT [52]	2.777	-0.2469	1.1907	-	-	0.3882
	MQ-MLPG1 ( $K = 1$ )	1.957	-0.2360	1.1700	0.0321	0.0110	0.3110
	MQ-MLPG1 ( $K = 3$ )	2.015	-0.2470	1.2000	0.0340	0.0118	0.4100
	MQ-MLPG1 ( $K = 5$ )	2.028	-0.2490	1.2100	0.0338	0.0118	0.4880
	TPS-MLPG1 ( $K = 1$ )	1.958	-0.2360	1.1800	0.0337	0.0111	0.3370
	TPS-MLPG1 ( $K = 3$ )	2.016	-0.2470	1.2000	0.0345	0.0119	0.4370
	TPS-MLPG1 ( $K = 5$ )	2.028	-0.2490	1.2100	0.3370	0.0119	0.4990

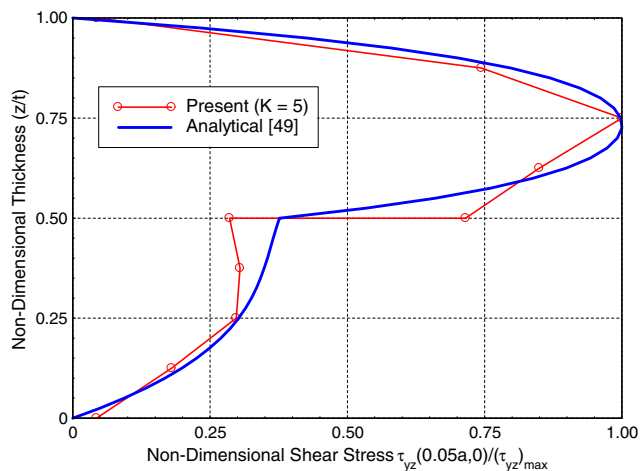


Fig. 8. Through-the-thickness variations of shear stress ( $\tau_{yz}$ ) in the  $0^\circ/90^\circ$  laminated plate computed with the present method and the analytical solution [49].

and  $0.246q$  with  $K = 3, 5$  and  $7$ , respectively. The presently computed through-the-thickness distribution of  $\bar{\tau}_{yz}$  agrees well with that obtained from the analytical solution except at the interface, where the stress from the analytical solution is continuous across the interface but that from the present solution is discontinuous. This suggests that one should either use the method of Lagrange multipliers, or the penalty method, or adopt another technique to ensure the continuity of tractions across an interface; this is left for a future study.

## 8. Conclusions

The higher order shear and normal deformable plate theory (HOSNDPT) has been combined with the meshless local Petrov–Galerkin (MLPG) method using radial basis functions (RBFs) to analyze static infinitesimal deformations of laminated elastic plates. Two types of RBFs, multiquadrics (MQ) and the thin plate splines (TPS), have been employed to approximate the trial solution and the 4th order spline function is used as the test function. The fully converged numerical solution is computed with  $13 \times 13$  uniformly spaced nodes on the mid-surface of the laminate. An advantage of using RBFs is that the corresponding shape functions possess the Kronecker delta property; therefore it is easy to impose the essential boundary conditions and the computational cost is substantially reduced.

Computed results for different laminates with either uniformly distributed or sinusoidally varying load on the top surface are found to match well with those obtained from the analysis of the corresponding 3D problems. All components of the stress tensor, including the transverse stresses, are computed from equations of the plate theory. It is found that deflections and stresses computed at interior points of the plate are in good agreement with those obtained from the analysis of the 3D problem which is regarded as the reference solution. However, transverse shear stresses computed at points on the plate edges differ somewhat from

those in the reference solution. The present study suggests that at least a third-order shear and normal deformable plate theory is required to compute accurate values of deflection, in-plane axial stresses and transverse stresses. It should be noted that other plate theories neglect the effect of transverse normal deformation, and good values of transverse stresses are obtained by integrating through-the-thickness the balance of linear momentum. In addition, the numerical solution obtained with the MLPG1 method using RBFs and  $13 \times 13$  uniformly spaced nodes on the midsurface and  $K = 5$  is as accurate as the solution of the 3D elasticity problem computed with the finite element method employing 4800 elements. The total number of degrees of freedom in the MLPG1 and the finite element methods equals  $169 \times 6 \times 3 = 3042$  and  $21 \times 21 \times 13 \times 3 = 18759$ , respectively. Thus the present method is computationally more efficient than the finite element method. Furthermore, there is no element connectivity required which reduces the effort required to prepare the input file.

## Acknowledgements

D.F.G. acknowledges the support of the Irish Research Council for Science, Engineering and Technology Post-graduate Scholarship scheme to the University of Limerick, and the Internship from the University of Delaware Center for Composite Materials. R.C.B.'s work was partially supported by the ONR Grant N00014-1-06-0567 to Virginia Polytechnic Institute and State University with Dr. Y.D.S. Rajapakse as the Program Manager. Views expressed herein are those of authors and neither of funding agencies nor of authors' institutions.

## References

- [1] Lo KH, Christensen RM, Wu EM. A higher-order theory of plate deformation. *J Appl Mech* 1997;44:663–76.
- [2] Phan ND, Reddy JN. Analysis of laminated composite plates using a higher-order shear deformation theory. *Int J Num Meth Eng* 1985;21:2201–19.
- [3] Batra RC, Vidoli S. Higher-order piezoelectric plate theory derived from a three-dimensional variational principle. *AIAA J* 2002;40:91–104.
- [4] Kocak S, Hassis H. A higher order shear deformable finite element for homogeneous plates. *Eng Struct* 2003;25:131–9.
- [5] Batra RC, Aimmanee S. Vibrations of thick isotropic plates with higher order shear and normal deformable plate theories. *Comput Struct* 2005;83:934–55.
- [6] Batra RC, Vidoli S, Vestroni F. Plane wave solutions and modal analysis in higher order shear and normal deformable plate theories. *J Sound Vibration* 2004;257:63–88.
- [7] Qian LF, Batra RC, Chen LM. Elastostatic deformations of a thick plate by using a higher-order shear and normal deformable plate theory and two meshless local Petrov–Galerkin (MLPG) methods. *CMES – Comput Model Eng Sci* 2003;4:161–76.
- [8] Qian LF, Batra RC, Chen LM. Static and dynamic deformations of thick functionally graded elastic plate by using higher-order shear and normal deformable plate theory and meshless local Petrov–Galerkin method. *Compos B* 2004;35:685–97.
- [9] Qian LF, Batra RC. Transient thermoelastic deformations of a thick functionally graded plate. *J Therm Stress* 2004;27:705–40.

- [10] Belytschko T, Lu YY, Gu L. Element-free Galerkin methods. *Int J Num Meth Eng* 1994;37:229–56.
- [11] Liu WK, Jun S, Zhang Y. Reproducing kernel particle methods. *Int J Num Meth Fluids* 1995;20:1081–106.
- [12] Duarte CA, Oden JT. An h-p adaptive method using clouds. *Comput Meth Appl Mech Eng* 1996;139:237–62.
- [13] Babuska I, Melenk J. The partition of unity method. *Int J Num Meth Eng* 1997;40:727–58.
- [14] Atluri SN, Zhu T. A new meshless local Petrov–Galerkin (MLPG) approach in computational mechanics. *Computat Mech* 1998;22:117–27.
- [15] Atluri SN, Zhu T. The meshless local Petrov–Galerkin (MLPG) approach for solving problems in elasto-statics. *Computat Mech* 2000;25:169–79.
- [16] Atluri SN, Shen S. The meshless local Petrov–Galerkin (MLPG) method. Tech Science Press; 2002.
- [17] Lucy LB. A numerical approach to the testing of the fission hypothesis. *Astron J* 2000;82:1013–24.
- [18] Zhang GM, Batra RC. Modified smoothed particle hydrodynamics method and its application to transient problems. *Computat Mech* 2004;34:137–46.
- [19] Han ZD, Liu HT, Rajendran AM, Atluri SN. The applications of meshless local Petrov–Galerkin (MLPG) approaches in high-speed impact, penetration and perforation problems. *CMES – Comput Model Eng Sci* 2006;14:119–28.
- [20] Batra RC, Porfiri M, Spinello D. Analysis of electrostatic MEMS using meshless local Petrov–Galerkin (MLPG) method. *Eng Anal Boundary Elements* 2006;30:949–62.
- [21] Hardy RL. Multiquadric equations of topography and other irregular surfaces. *J Geophys Res* 1971;76:1905–15.
- [22] Kansa EJ. Multiquadrics – a scattered data approximation scheme with application to computational fluid-dynamics—I and II. *Comput Math Appl* 1990;19:127–61.
- [23] Golberg MA, Chen CS, Karur SR. Improved multiquadric approximation for partial differential equations. *Eng Anal Boundary Elements* 1996;18:9–17.
- [24] Fasshauer GE. Solving partial differential equations by collocation with radial basis functions. In: Le Méhauté A, Rabut C, Schumaker LL, editors. *Surface Fitting and Multiresolution Methods*. Nashville, TN: Vanderbilt University Press; 1997. p. 131–8.
- [25] Wendland H. Meshless Galerkin method using radial basis functions. *Math Comput* 1999;68:1521–31.
- [26] Liu GR, Gu YT. A local radial point interpolation method (LRPIM) for free vibration analysis of 2-D solids. *J Sound Vibration* 2001;246:29–46.
- [27] Wang JG, Liu GR. On the optimal shape parameters of radial basis functions used for 2-D meshless methods. *Comput Meth Appl Mech Eng* 2002;191:2611–30.
- [28] Xiao JR, McCarthy MA. A local Heaviside weighted meshless method for two-dimensional solids using radial basis functions. *Computat Mech* 2003;31:301–15.
- [29] Xiao JR, Gama BA, Gillespie Jr JW, Kansa EJ. Meshless solutions of 2D contact problems by subdomain variational inequality and MLPG method with radial basis functions. *Eng Anal Boundary Elements* 2005;29:95–106.
- [30] Belinha J, Dinis LMJS. Analysis of plates and laminates using the element-free Galerkin method. *Comput Struct* 2006;84:1547–59.
- [31] Peng LX, Kitipornchai S, Liew KM. Analysis of rectangular stiffened plates under uniform lateral load based on FSDT and element-free Galerkin method. *Int J Mech Sci* 2005;47:251–76.
- [32] Wang J, Liew KM, Tan MJ, Rajendran S. Analysis of rectangular laminated composite plates via FSDT meshless method. *Int J Mech Sci* 2002;44:1275–93.
- [33] Ferreira AJM. A formulation of multiquadric radial basis function method for the analysis of laminated composite plates. *Compos Struct* 2003;59:385–92.
- [34] Ferreira AJM, Roque CMC, Martins PALS. Analysis of composite plates using higher order shear deformation theory and a finite point formulation based on the multiquadric radial basis function method. *Compos B* 2003;34:627–36.
- [35] Ferreira AJM, Roque CMC, Jorge RMN. Analysis of composite plates by trigonometric shear deformation theory and multiquadrics. *Comput Struct* 2005;83:2225–37.
- [36] Xiao JR, Batra RC, Gilhooly DF, Gillespie Jr JW, McCarthy MA. Analysis of thick plates by using a higher-order shear and normal deformable plate theory and MLPG method with radial basis functions. *Comput Meth Appl Mech Eng* 2007;196:979–87.
- [37] Gilhooly DF, Batra RC, Xiao JR, McCarthy MA, Gillespie Jr JW. Analysis of thick functionally graded plates by using higher-order shear and normal deformable plate theory and MLPG method with radial basis functions. *Compos Struct*, in press.
- [38] Qian LF, Batra RC, Chen LM. Free and forced vibrations of thick rectangular plates by using higher-order shear and normal deformable plate theory and meshless Petrov–Galerkin (MLPG) method. *Comput Model Eng Sci* 2003;4:519–34.
- [39] Qian LF, Batra RC, Chen LM. Analysis of cylindrical bending thermoelastic deformations of functionally graded plates by a meshless local Petrov–Galerkin method. *Computat Mech* 2004;33:263–73.
- [40] Qian LF, Batra RC. Design of bidirectional functionally graded plate for optimal natural frequencies. *J Sound Vibration* 2005;280:415–24.
- [41] Qian LF, Batra RC. Three-dimensional transient heat conduction in a functionally graded thick plate with a higher-order plate theory and a meshless local Petrov–Galerkin method. *Computat Mech* 2005;35:214–26.
- [42] Kapuria S, Achary GGS. Nonlinear zigzag theory for electromechanical buckling of piezoelectric composite and sandwich plates. *Acta Mech* 2006;184:61–76.
- [43] Kapuria S, Alam N. Efficient layerwise finite element model for dynamic analysis of laminated piezoelectric beams. *Comput Meth Appl Mech Eng* 2006;195:2742–60.
- [44] Kapuria S. A coupled zig-zag third-order hybrid cross-ply plates. *J Appl Mech* 2004;71:604–14.
- [45] Reddy JN. *Mechanics of laminated composite plates*. CRC press; 1996.
- [46] Reddy JN. A simple higher-order theory for laminated composite plates. *J Appl Mech* 1984;51:745–52.
- [47] Pagano NJ. Exact solutions for rectangular bidirectional composites and sandwich plates. *J Compos Mater* 1970;4:20–34.
- [48] Ferreira AJM, Roque CMC, Martins PALS. Radial basis functions and higher order shear deformation theories in the analysis of laminated composite beams and plates. *Compos Struct* 2004;66:287–93.
- [49] Vel SS, Batra RC. Analytical solutions for rectangular thick laminated plates subjected to arbitrary boundary conditions. *AIAA J* 1999;37:1464–73.
- [50] Vel SS, Batra RC. The generalized plane strain deformations of thick anisotropic composite laminated plates. *Int J Solid Struct* 2000;37:715–33.
- [51] Vel SS, Batra RC. Closure to the generalized plane strain deformations of thick anisotropic composite laminated plates. *Int J Solid Struct* 2000;38:483–9.
- [52] Khdeir AA, Reddy JN. Analytical solutions of refined plate theories of cross-ply composite laminates. *J Pressures Vessel Tech* 1991;113(4):570–8.